



AMERICAN
SCIENTIFIC
PUBLISHERS

Copyright © 2019 American Scientific Publishers
All rights reserved
Printed in the United States of America

DNA Nanorobot Delivers Antisense Oligonucleotides Silencing c-Met Gene Expression for Cancer Therapy

Xiaolin Zhang^{1,†}, Nanxin Liu^{1,†}, Mi Zhou¹, Tao Zhang¹, Taoran Tian¹, Songhang Li¹, Zisheng Tang², Yunfeng Lin¹, and Xiaoxiao Cai^{1,*}

¹State Key Laboratory of Oral Diseases, National Clinical Research Center for Oral Diseases, West China Hospital of Stomatology, Sichuan University, Chengdu 610041, P. R. China

²Department of Endodontics, Shanghai Ninth People's Hospital, College of Stomatology, Shanghai Jiao Tong University School of Medicine, Shanghai 200011, P. R. China

Antisense oligonucleotides are considered to be a promising strategy for cancer therapy because of their high specificity and minimal side effects. They can bind specifically to mRNA silencing the expression of target genes. However, ssDNA cannot enter cells in large quantities, which limits its applications. Tetrahedral framework nucleic acids (tFNA) are considered to be optimal nanoscopic drug carriers because of their editability and biocompatibility. Most importantly, they can be modified with functional molecules. The over-expression of c-Met is associated with a wide variety of tumor occurrences, developments, drug resistance and prognoses. Activation of HGF/c-Met signaling pathways can promote cell migration and invasion in cancer. Therefore, blocking the expression of c-Met is a valid technique for cancer therapy. In this study, we used tFNA as carriers to deliver antisense oligonucleotides, which can bind to c-Met mRNA with high specificity and affinity, into cells resulting in the inhibition of c-Met expression for cancer therapy.

KEYWORDS: tFNA, Antisense Oligonucleotides, Cell Migration, HGF/c-Met Signaling Pathway, Cancer Therapy.

INTRODUCTION

In recent years, treatment of malignant tumors has entered an era of individualization and molecular targeting. Therefore, new individual-based treatments for cancer patients has been a top priority. Antisense oligonucleotides (ANOs) are single-stranded DNA or RNA, which work by binding to target mRNA through the principles of Watson-Crick base pairing to block the translation of mRNA; therefore, ANOs are agents that are highly specific and have minimal side effects [1–2]. The use of ANOs to silence gene expression is considered to be a promising strategy for cancer treatment [3–4].

Because cancer cells can migrate from primary lesions to other organs, cancer is an elusive therapeutic target [5–6]. Research shows that, HGF/c-Met signaling pathways are involved in metastasis and the proliferation, migration and morphological changes of various cancer

cells; they lead to tumor invasion, migration, and finally angiogenesis [7–9]. The over-expression of c-Met is associated with tumor occurrence, development, invasion, metastasis, prognosis and drug resistance [10]. HGF and its receptor c-met take an important part in the progression of various tumors, such as thyroid cancer, head and neck squamous cell carcinoma, digestive system tumor [7–9]. Therefore, c-Met is a promising target for tumor treatment, and studies of its inhibitors have become a popular research topic [11–13].

To block c-Met expression and subsequent cellular signaling, in this study, we designed ANOs that can bind to c-Met mRNA with high specificity and affinity, resulting in the inhibition of c-Met expression. However, because they are easily degraded by nucleases and it is difficult for them to enter cells, ANOs cannot play an effective role in silencing gene expression alone [14–17]. Therefore, a drug carrier is needed.

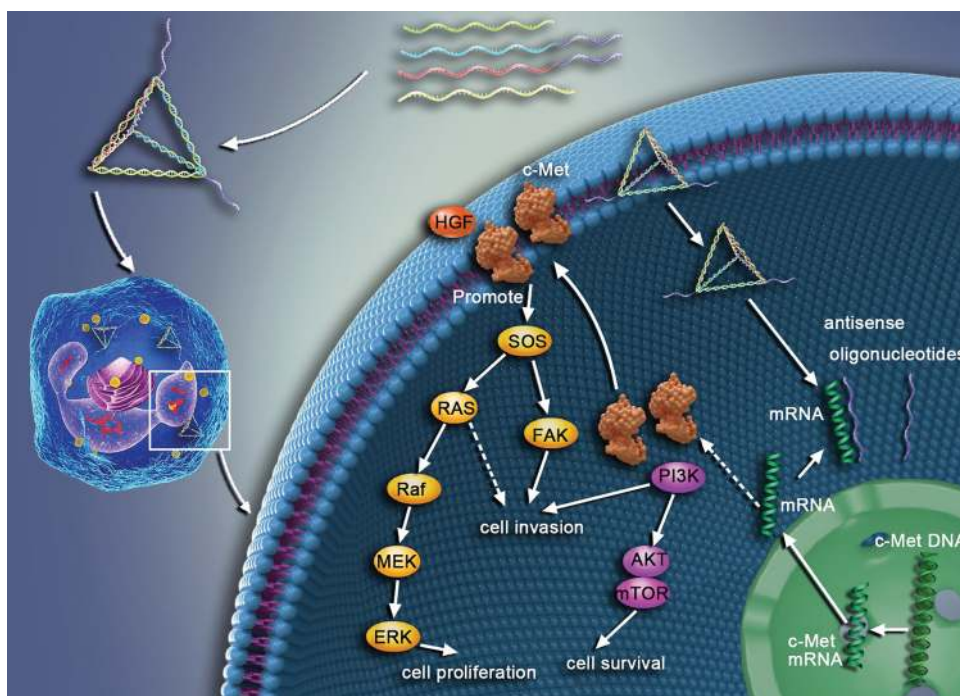
For the past few years, DNA nanomaterials have been widely applied to all aspects of biomedicine, including bioimaging, molecular transport, molecular diagnosis, and targeted drug delivery [18–28]. Among various DNA

*Author to whom correspondence should be addressed.
Email: xcai@scu.edu.cn

[†]These two authors contributed equally to this work.

Received: 14 March 2019

Accepted: 7 May 2019



Scheme 1. Schematic illustration of the synthesis of ANOs-tFNA complex, and the way it blocks the expression of c-Met gene.

nanostructures, tFNA are a major research focus because of their exceptional mechanical rigidity, structural stability, and versatility regarding modification. According to previous articles [29–37], tFNA are a new kind of nanomaterial composed of four single-stranded DNA at a high yield. Because of their biocompatibility, biodegradability and the ability to penetrate cellular membrane, tFNA have been widely used in all aspects of biomedicine. The other advantage of tFNA is their high biological safety, attributable to the biological nature of DNA, which can be degraded by cells [34–41]. Most importantly, they can be modified by many kinds of functional molecules, such as nucleic acids, aptamers, peptides, and antibodies [20–22]. Studies have shown that tFNA can protect single-strand sequences against nuclease degradation [21–24]. Therefore, we assume that tFNA can be modified with functional ANOs, forming a novel targeted delivery system to regulate cell behavior [41–44]. In this article, ANOs, which can specifically bind to c-Met mRNA to block HGF/c-Met signaling pathway and finally inhibit tumor migration and proliferation, were delivered by tFNA to enter cells (Scheme 1).

EXPERIMENTAL DETAILS

Design of Antisense Oligonucleotides Targeting c-Met mRNA

We searched the sequence of c-Met mRNA using the National Center for Biotechnology Information (NCBI, NM000245). Antisense oligonucleotide chains were designed according to the selected target sequences,

and the three sequences of c-Met mRNA selected are listed in Table I. Furthermore, blast homology analysis was used to ensure the specificity of gene inhibition. A randomized control sequence was designed, that was not homologous to any human gene sequence according to the blast homology analysis. Except for the randomized control sequence, each antisense oligonucleotide was added to the 5' end of S2 and S3 (Table II).

Cell Culture and Grouping

According to previous research, c-Met is over-expressed in esophageal cancer cells [45–49]. Human esophageal cancer cell line TE10 cells acquired from Shanghai Guandao Biological Engineering Company (Shanghai, China), were cultured in high-glucose DMEM in which the concentration of fetal bovine serum (FBS) was 10% and the concentration of penicillin–streptomycin solution was 1%; they were then placed in a moist environment at 37 °C and 5% CO₂. First, we selected the best concentration of tFNA, and five groups were established according to the concen-

Table I. Base sequence of each single-stranded DNA (ssDNA) of target gene.

ssDNA	Direction	Base sequence
cMet1	5'-3'	GTATCAGCTTCCCAACTTCACCG
Antisense	3'-5'	CATAGTCGAAGGGTTGAAGTGGC
cMet2	5'-3'	GCAAGCCAGATTCTGCCGAACCA
Antisense	3'-5'	CGTTCCGGTCTAAGACGGCTTGGT
cMet3	5'-3'	GGAGGGACAAGGCTGACCATATG
Antisense	3'-5'	CCTCCCTGTTCCGACTGGTATAC

Table II. Base sequence of ssDNA modified with ANOs.

ssDNA	Direction	Base sequence
cMet1-S2	5'-3'	CGGTGAAGTTGGGAAGCTGATACT TTTTACATGCGAGGGTCCAATACC GACGATTACAGCTTGCTACAC GATTCAGACTTAGGAATGTTTCG
cMet1-S3	5'-3'	CGGTGAAGTTGGGAAGCTGATACT TTTTACTACTATGGCGGGTG ATAAAACGTGTAGCAAGCTGTAA TCGACGGGAAGAGCATGCCCATCC
cMet2-S2	5'-3'	TGGTTCGGCAGAATCTGGCTTGCT TTTTACATGCGAGGGTCCAA TACCGACGATTACAGCTTGCTAC ACGATTACAGCTTAGGAATGTTTCG
cMet2-S3	5'-3'	TGGTTCGGCAGAATCTGGCTTGCT TTTTACTACTATGGCGGGT GATAAAACGTGTAGCAAGCTGTAAT CGACGGGAAGAGCATGCCCATCC
cMet3-S2	5'-3'	CATATGGTCAGCCTTGTCCTCC TTTTACATGCGAGGGTCCAATA CCGACGATTACAGCTTGCTACAC GATTCAGACTTAGGAATGTTTCG
cMet3-S3	5'-3'	CATATGGTCAGCCTTGTCCTCC TTTTACATGCGAGGGTCCAATA CCGACGATTACAGCTTGCTACA CGATTACAGCTTAGGAATGTTTCG

tration of tFNA (0, 125, 250, 375, and 500 nM). Second, to make the research more efficient, we selected the sequence with the most significant inhibitory effect. Five groups were set, and each group was treated with various drugs at the same concentration (Control, treated with TM buffer; tFNA-cMet1, tFNA modified with antisense sequence1; tFNA-cMet2, tFNA modified with antisense sequence2; tFNA-cMet3, tFNA modified with antisense sequence3). Finally, to prove that tFNA, as a carrier, can improve the cellular uptake efficiency of ANOs, we set up four groups treated with various drugs at the same concentration (A: Control, treated with TM buffer; B, tFNA, treated with tFNA; C, c-Met, treated with the ANOs selected as the most efficient; D, tFNA-cMet, treated with tFNA modified with ANOs that proved to be the most efficient).

Synthesis of tFNA and the ANOs-tFNA Complex

tFNA were synthesized as previously reported [24–37]: First, four specific ssDNA (S1, S2, S3 and S4, listed in Table III) were equally mixed in TM buffer. The synthesis conditions are as follows: 10 min at 95 °C, then cooled down to 4 °C for 20 min. The ANOs-tFNA complex was prepared under the same conditions to synthesize tFNA with antisense oligonucleotides added to the 5' end of S2 and S3.

Characterization of tFNA and the ANOs-tFNA Complex

The successful synthesis of DNA nanostructures can be detected by various techniques, such as transmission electron microscopy (TEM, Hitachi, HT7700, Japan),

polyacrylamide gel electrophoresis (PAGE, 8%), and dynamic light scattering (DLS) [24–33]. First, we used PAGE to verify that tFNA and the ANOs-tFNA complex were synthesized successfully. The PAGE technique separates DNA molecules by size, which mean that the shorter moved faster and the longer structures moved slower [34–36]. When the DNA nanoparticles were modified with ANOs, the DNA exhibited a lower gel mobility than the tFNA before modification, indicating that the ANOs-tFNA complex was synthesized successfully. For further confirmation, TEM was used to observe the structure and morphology of tFNA and the ANOs-tFNA complex. In addition, DLS was used to measure the size of tFNA and the ANOs-tFNA complex.

Cellular Uptake of tFNA and the ANOs-tFNA Complex

Cellular uptake of tFNA and the ANOs-tFNA complex was analyzed using flow cytometry and a confocal microscope (Leica, Wetzlar, Germany). First, to confirm that tFNA and the ANOs-tFNA complex enter cells successfully, flow cytometry was performed. Seeded in six-well plates (2×10^5 /well), TE10 cells were cultured in regular medium until the cells adhered to the wall, after which the cells were cultured in medium without FBS but containing tFNA (Cy5-TDNs, 250 nM) and the ANOs-tFNA complex (Cy5-ANOs-tFNA complex, 250 nM) modified with Cyanine-5 (Cy5). After incubation for 12 h, the cells were collected. A flow cytometer (FC500 Beckman, IL, USA) was used to measure the percentage of cells that contained Cy5 to analyze the cellular uptake. Furthermore, we observed the localization of DNA nanoparticles in cells using fluorescence-based assays. To prove that tFNA and the ANOs-tFNA complex can enter TE10 cells, cells were incubated with tFNA (Cy5-TDNs, 250 nM) and the ANOs-tFNA complex (Cy5-ANOs-tFNA complex, 250 nM) modified with Cy5 for 12 h. After being washed by PBS for thrice (5 min at a time), the samples were fixed in 4% cold paraformaldehyde solution for 30 min. After that,

Table III. Base sequence of each single-stranded DNA (ssDNA).

ssDNA	Direction	Base sequence
S1	5'-3'	ATTTATCACCCGCCATAGTAGACG TATCACCAGGCAGTTGAGACGA ACATTCTAAGTCTGAA
S2	5'-3'	ACATGCGAGGGTCCAATACCGACG ATTACAGCTTGCTACACGATT CAGACTTAGGAATGTTTCG
S3	5'-3'	ACTACTATGGCGGGTGATAAAACGT GTAGCAAGCTGTAATCGACGG GAAGAGCATGCCCATCC
S4	5'-3'	ACGGTATTGGACCCTCGCATGACT CAACTGCCTGGTGATACGAGGA TGGGCATGCTCTTCCCG

the nuclei and cytoskeleton were stained with DAPI and FITC-labeled phalloidin. Finally, we used a confocal laser microscope to observe any fluorescent substance inside the cells and to capture cell images.

Cell Proliferation Assay

Real-time cell analysis (RTCA) and CCK-8 were performed to analyze cell proliferation. After selecting the optimal concentration of drugs and the most efficient sequence, there were four groups: A: Control (TMBuffer, 250 nM); B: tFNA (tFNAs, 250 nM); C: c-Met (the ANOs that were the most efficient, 250 nM); D: tFNA-cMet (tFNA modified with ANOs that were the most efficient at blocking c-Met gene expression, 250 nM). For CCK-8, TE10 cells were placed in 96-well plates (4×10^3 /well) in regular medium and cultured until the cells adhered to the wall. Then, the regular medium was changed to one containing various drugs at the same concentration without FBS. Finally, the cells were collected at different points in time (24 h, 48 h, and 72 h) to test the cell proliferation with CCK-8 solution. For RTCA, first, TE10 cells were placed in sixteen-well plates (4×10^3 /well) that were matched with the testing instrument, and cultured in regular medium until the cells adhered to the wall. Then, the cells were incubated with various drugs without FBS. Cell proliferation was monitored in real time using an RTCA instrument (xCELLigence, Roche Diagnostics, Switzerland).

Apoptosis and Cell Cycle Assay

To confirm that tFNA can help deliver the ANOs in cells and to test the effects of the ANOs on cells, flow cytometry was performed to analyze cell apoptosis and the cell cycle. The previous steps of these two tests were the same. First, the cells were cultured in regular medium in six-well plates. Then, the regular medium was changed to a medium containing various drugs. Cells were collected at 48 h and treated with the appropriate kit. Finally, the cells were measured by a flow cytometer to analyze apoptosis and the cell cycle.

Cell Migration/Invasion Assays

As previously mentioned, c-Met, as the receptor of HGF, takes an important part in the metastasis and invasion of tumor cells [6–12]. To confirm that the ANOs-tFNA complex can down-regulate the expression of c-Met, block the HGF/c-Met signaling pathway, and inhibit cell migration, we performed RTCA and Cell Migration-Transwell chamber Assays. The principles of the two techniques are the same. In RTCA, there are two chambers in each well: the upper chamber and the lower chamber. The upper chamber contained medium without FBS and various drugs. The lower chamber, contained regular medium. Because the lower chamber was more favorable for cell growth, cells were promoted to migrate to the lower chamber. Briefly

speaking, TE10 cells were seeded in the bottom of the upper chamber, which contained a PET membrane with 8 mm pores. After incubation for 24 h, the cells moved through the pores to the other side of the membrane. Then, the cells that moved through the pores were stained with DAPI and observed. We compared the effects of different groups by counting the number of migrated cells.

Immunofluorescence Staining

To detect cell apoptosis, apoptosis-related proteins were examined using a confocal laser microscope. The proteins examined were c-Met, Bax, Caspase-3, and Bcl-2 [48–49]. After treatment with various drugs for 48 h, the samples were washed with PBS for thrice, fixed with cold paraformaldehyde (4%) for 30 min, then permeabilized by 0.5% Triton X-100 for 10 min, and then blocked with 5% sheep serum for 1 h at room temperature. Then, the samples were probed with primary antibodies specific to Bcl-2, c-Met, Bax, or Caspase-3 (1:500, Abcam, UK) diluted in PBS overnight at 4 °C. Next, a fluorescent secondary antibody (1:200) was used to incubate the samples at 37 °C for 1 h. After that, the nuclei and cytoskeleton were stained with DAPI and FITC-labeled phalloidin. Finally, a confocal laser microscope was used to observe the samples and acquire images.

Western Blot Analysis

The expressions of c-Met, Bax, Caspase-3, and Bcl-2 were examined by Western Blotting. The TE10 cells were collected, after the samples were treated with DMEM containing various drugs for 48 h. After the samples were washed with PBS three times, a whole protein extraction kit (KeyGEN BioTECH, Nanjing, China) was used to extract total proteins from cells. A 5× loading buffer was mixed with the protein samples in appropriate proportion; after that, the mixture was boiled for 5 min. Various gel concentrations of sodium dodecyl sulfate-PAGE were used to separate the targeted proteins at 100 V for 90 min. Then, the separated proteins were transferred to a PVDF membrane. Following incubation in blocking buffer for 1 h, the membranes were probed with primary antibodies specific to c-Met (1:1000), Bcl-2 (1:1000), Bax (1:500), Caspase-3 (1:1000), and GAPDH (1:3000) (rabbit mAb, all from Abcam) overnight at 4 °C, washed by TBST three times (15 min at a time), then probed with a secondary antibody (1:3000, SAB, China) for 1 h. After washed with TBST for three times again, every membrane was visualized by an enhanced chemiluminescence reagent. Moreover, because of its stable expression, GAPDH was used as the internal control.

Quantitative Polymerase Chain Reaction

The mRNA levels of c-Met, Bax, and Caspase-3 were measured by quantitative PCR (mRNA primer pair sequences are listed in Table IV). After the cells were

Table IV. Primer sequences of relevant genes designed for qPCR.

mRNA	Primer pairs
GAPDH	Forward 5'-AGAGGGATGCTGCCCTTACC-3' Reverse 5'-ATCCGTTACACCGACCTTC-3'
c-Met	Forward 5'-CAGGACCATCAACCCCTCAT-3' Reverse 5'-CACACTGAACAAAGGGTGGG-3'
Bax	Forward 5'-TCATGGGCTGGACATTGGAC-3' Reverse 5'-GAGACAGGGACATCAGTCGC-3'
Caspase-3	Forward 5'-GCGGTTGTAGAAGTTAATAAAGGTA-3' Reverse 5'-CATGGCACAAAGCGACTGG-3'

treated with various drugs for 24 h, the cells were lysed by Trizol (Thermo Fisher Scientific, MA, USA) to extract total RNA. A synthesis kit was used to reverse transcribe every RNA sample into cDNA (PrimeScript™ RT reagent Kit, Takara, Japan). To evaluate the expression of target mRNAs in each sample, target cDNA was amplified in a QuantStudio3 Thermal Fisher cyclor (Applied Biosystems, Foster City, CA) using TB Green II (Takara, Japan). In addition, GAPDH was used as an internal parameter to evaluate the expression of target genes.

Statistical Analysis

All experiments were performed at least thrice. Student's *t*-test and one-way analysis of variance were performed to analyze data. **p* < 0.05, ***p* < 0.01, and ****p* < 0.001 indicate significant results. Quantitative results are presented as the mean ± standard deviation (SD) with *n* ≥ 3 replicates.

RESULTS AND DISCUSSION

Synthesis and Characterization of tFNA and the ANOs-tFNA Complex

tFNA were synthesized of four ssDNA using a thermal cyclor (Bio-Rad, Hercules, CA) (Fig. 1(A)). To construct the ANOs-tFNA complex, an antisense oligonucleotide targeting c-Met mRNA, which has been proven to inhibit cell proliferation and migration, was added to the 5' end of S2 and S3. The PAGE technique was used to verify the successful synthesis of tFNA and the ANOs-tFNA complex according to previous reports. SsDNA moved faster than tFNA, and tFNA moved faster than the ANOs-tFNA complex, because of the extra added ANOs, which indicates

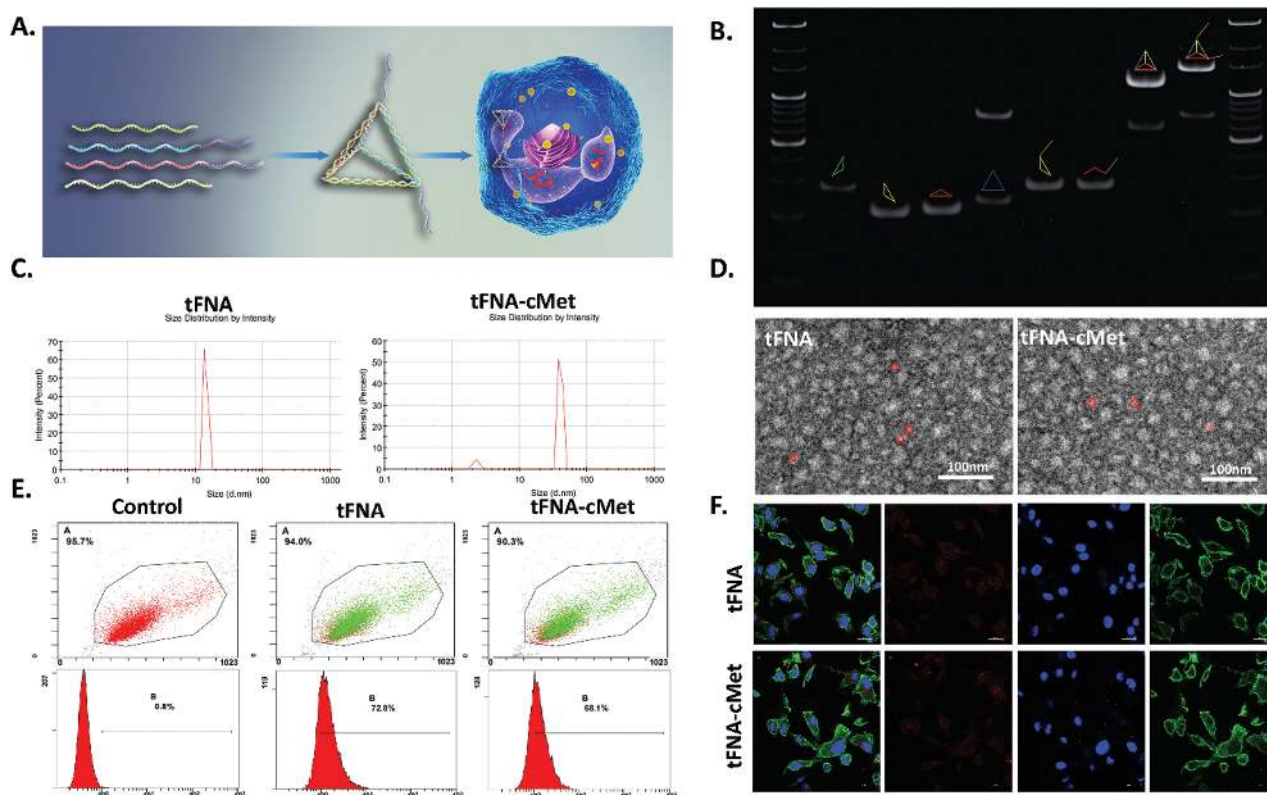


Figure 1. Characterizations and cellular uptake of tFNA and tFNA-ANOs complex. (A) An abridged general view of synthesis of tFNA-ANOs complex; (B) result of PAGE analysis indicated tFNA and tFNA-ANOs complex were synthesized successfully; (C) size of tFNA and tFNA-ANOs complex detected by dynamic light scattering; (D) the structure of tFNA and tFNA-ANOs complex observed with TEM intuitively; (E) flow cytometric analysis of cell uptake of Cy5-tFNA and Cy5-tFNA-ANOs complex; (F) images of TE10 cells taken with immunofluorescence microscope. (Nucleus: Blue, cytoskeleton: Green, and Cy5: Red). Scale bars are 25 μ m.

that tFNA and the ANOs-tFNA complex were synthesized successfully (Fig. 1(B)). Moreover, the sizes of tFNA and the ANOs-tFNA complex were detected by a DLS (Fig. 1(C)). The average size of tFNA was approximately 14 nm, and the ANOs-tFNA complex was larger than those of tFNA. To further confirm the successful synthesis of tFNA and the ANOs-tFNA complex, the morphologies of tFNA and the ANOs-tFNA complex were observed by TEM, and triangular shapes were observed (Fig. 1(D)). All of these results confirmed that the tFNA and the ANOs-tFNA complex were synthesized successfully.

Cellular Uptake of tFNA and the ANOs-tFNA Complex

As previously reported, tFNA can enter cells rapidly via caveolin-mediated endocytosis, but ssDNA cannot. Now that, the ANOs-tFNA complex had been shown to be successfully synthesized and tFNA could be taken up by cells, we assumed that, as a delivery, tFNA could deliver the ANOs into cells, meaning that the ANOs-tFNA complex can be taken up by cells. To prove the successful cellular uptake of the ANOs-tFNA complex, flow cytometry was performed. The results indicated that there were 70 percent of the cells contained Cy5-tFNA and the Cy5-ANOs-tFNA complex (Fig. 1(E)). In addition, to observe the uptake of tFNA and the ANOs-tFNA complex intuitively, cells were treated with Cy5-tFNA and the Cy5-ANOs-tFNA complex for 6 h, and a confocal microscope was used to observe the cellular uptake of tFNA and the ANOs-tFNA complex

(Fig. 1(F)). The images show that there was a large amount of Cy5-tFNA and the Cy5-ANOs-tFNA complex in the cytoplasm.

Effect of ANOs-tFNA Complex on Cell Proliferation

In order to investigate the influence of ANOs-tFNA complex on cell proliferation, CCK-8 and RTCA were performed. First, to select the optimal concentration of the ANOs-tFNA complex and eliminate the influence of tFNA, the cells were incubated with increasing tFNA concentration, ranging from 0 to 500 nM (Fig. 2(A)). The optimal concentration was determined to be 250 nM, in which the tFNA would not inhibit cell proliferation. As a result, in subsequent experiments, the concentration of drugs we used was 250 nM. To compare the effect of three ANOs, the cells were treated with various drugs (Groups: Control, tFNA, tFNA-cMet1, tFNA-cMet2, and tFNA-cMet3) at a concentration 250 nM, and detected cell proliferation at 48 h. The results indicated that the ANOs2 was the most efficient one (Fig. 2(A)). In subsequent experiments, all the ANOs used were ANOs2. In order to prove that tFNA could improve the cellular uptake of ANOs, CCK-8 was performed. There were four groups (A, Control, treated with TM buffer; B, tFNA, treated with tFNA; C, c-Met, treated with the ANOs selected as the most efficient; D, tFNA-cMet, treated with tFNA modified with the ANOs that were proved to be the most efficient). Results of CCK-8 indicated that, compared with the control group, the tFNA-cMet group can inhibited cell

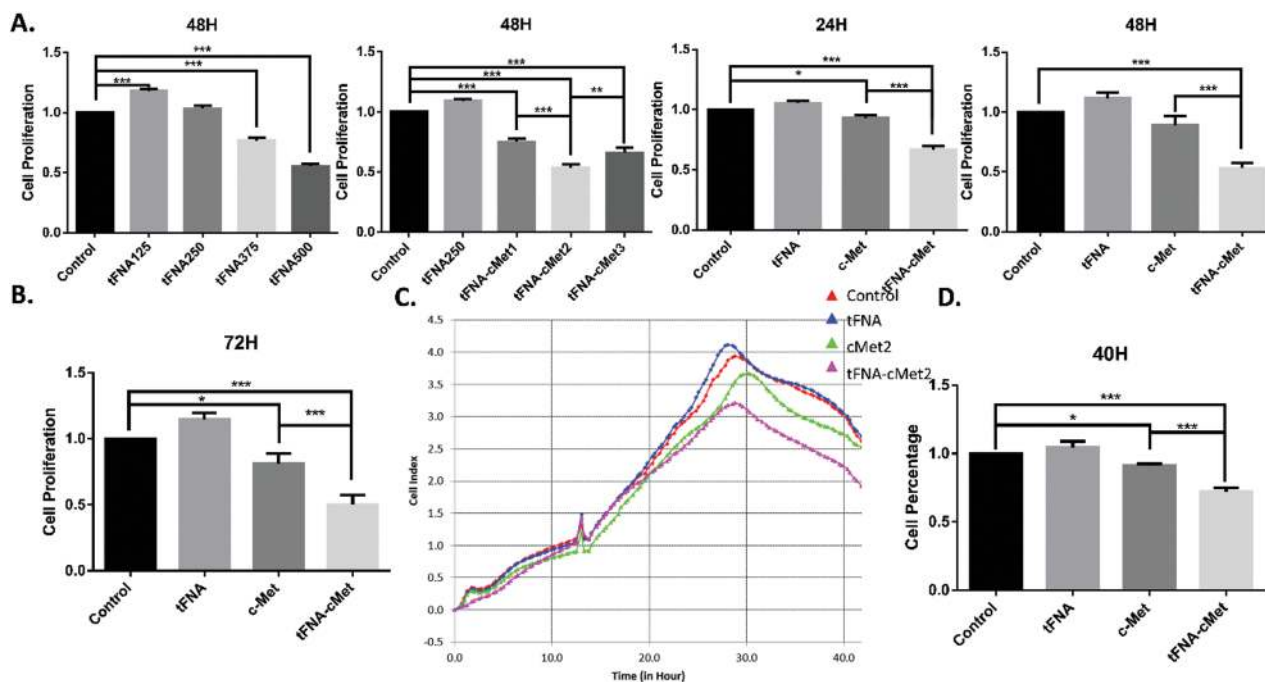


Figure 2. Effect of tFNA-ANOs complex on cell proliferation. (A, B) Cell proliferation analyzed by CCK-8 assay. Data are presented as mean \pm SD ($n = 4$). Statistical analysis: * $p < 0.05$, ** $p < 0.01$, and *** $p < 0.001$. (C, D) Cell proliferation was detected by RTCA system. Statistical analysis: * $p < 0.05$, ** $p < 0.01$, and *** $p < 0.001$.

proliferation significantly (Figs. 2(A, B)). To further confirm these results, RTCA was performed, and the growth curve indicated that cell proliferation for the tFNA-cMet group was inhibited significantly after drug treatment more than 30 h (Figs. 2(C, D)).

Effect of ANOs-tFNA Complex on TE10 Cell Apoptosis and Cell Cycle

As mentioned above, over-expression of c-Met can promote cell proliferation and migration. In order to prove that silencing the expression of c-Met can inhibit cell proliferation, flow cytometry was performed to measure

cell apoptosis. After treatment for 48 h, the percentage of late apoptotic cells and early apoptotic cells in the tFNA-cMet group was significantly higher than that in other groups (Figs. 3(A, C)). Moreover, flow cytometry was performed to detect the effect of the ANOs-tFNA complex on the cell cycle. As the results showed, the percentage of cells in the S phases of the tFNA-cMet group was decreased, compared with that of other groups. Meanwhile, tFNA-cMet caused an increase in the G2 phase (Figs. 3(B, D)). The change in cell cycle stage distribution indicated that ANOs targeting c-Met inhibited cell proliferation significantly.

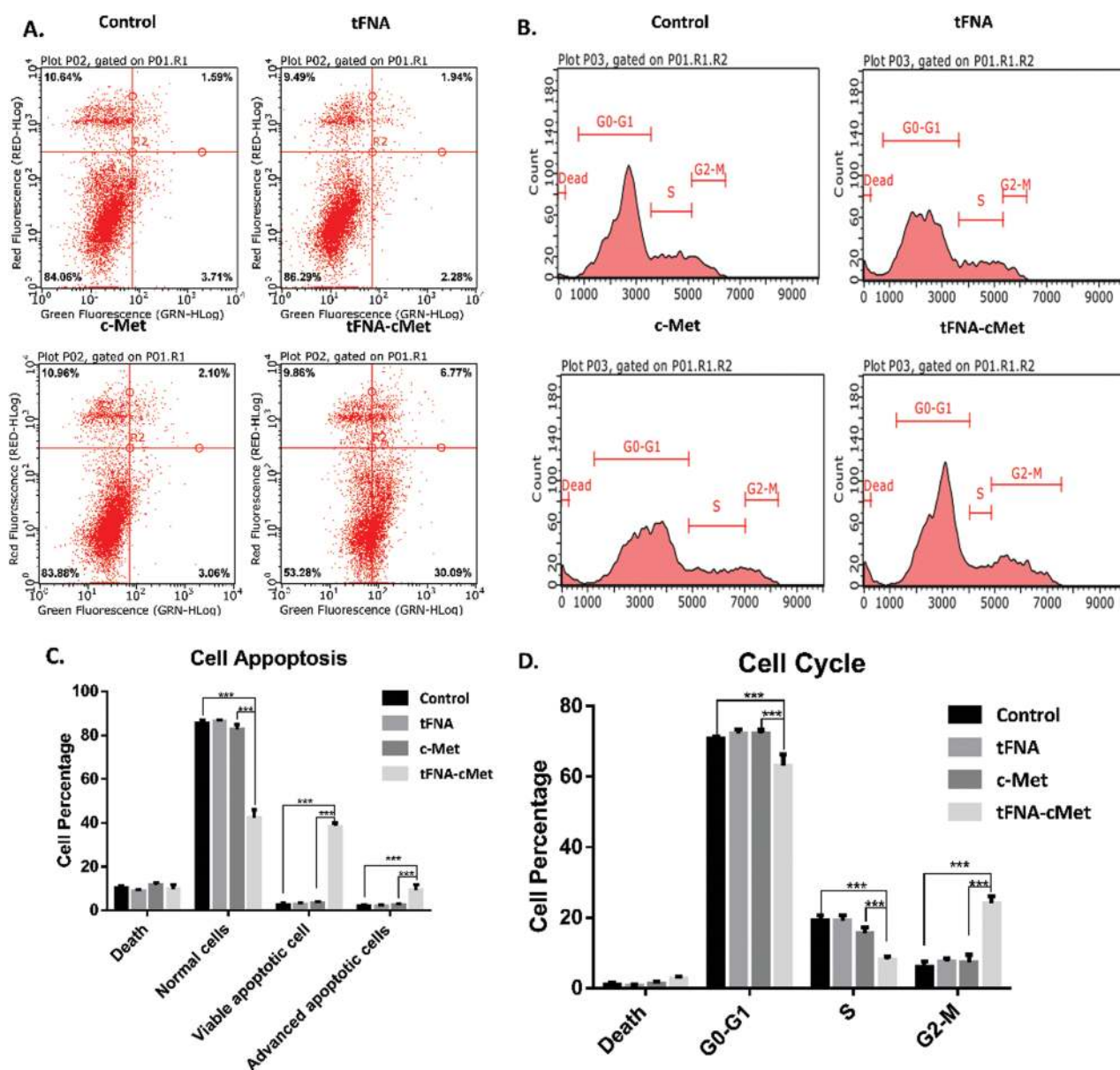


Figure 3. Effect of tFNA-ANOs complex on cell apoptosis, and cell cycle. (A, C) Flow cytometric examination and analysis of cell apoptosis. Statistical analysis: *** $p < 0.001$. (B, D) Cell cycle distribution analysis. Data are presented as mean \pm SD ($n = 4$). Statistical analysis: *** $p < 0.001$.

Effect of ANOs-tFNA Complex on TE10 Cell Migration

Transwell chamber assays were used to investigate the influence of the ANOs-tFNA complex on cell migration. The results showed that fewer cells were transferred to the other side of the membrane in the tFNA-cMet group than in other groups (Fig. 4(A)). In addition, quantitative analysis showed that the ANOs-tFNA complex markedly decreased the migration of TE10s ($***p < 0.001$; Fig. 4(B)). For further proof, RTCA was used to detect the invasiveness of TE10s. From Figure 4(C), we can conclude that the ANOs-tFNA complex significantly inhibited the cell migration of TE10s. The results of statistical analysis of the RTCA were the same (Fig. 4(D)). According to the results of RTCA and the transwell assay, migration of TE10s was obviously inhibited in the tFNA-cMet group.

Effect of ANOs-tFNA Complex on Expression of Related Proteins

To demonstrate that the ANOs-tFNA complex promoted cell apoptosis, an immunofluorescence assay was performed to observe the apoptosis-related protein-expression intuitively. As shown in Figures 5(A) and (B), after the

samples were exposed to the ANOs-tFNA complex for two days, the Bax and Caspase-3 fluorescent signals were much stronger than those in other groups. On the contrary, Figures 5(C) and (D) show much weaker c-Met and Bcl-2 fluorescent signals in tFNA-cMet groups than in other groups. Therefore, we conclude that the ANOs-tFNA complex could promote cell apoptosis by silencing c-Met. For further proof, Western blotting and an immunofluorescent assay were used to detect the expression of apoptosis-related proteins, such as Bax, Caspase-3, Bcl-2, and c-Met. The results indicate that Bax and Bcl-2 were over-expression in the group exposed to the ANOs-tFNA complex (Fig. 6(B)). By contrast, the expression of c-Met and Bcl-2 was reduced in the tFNA-cMet group compared with other groups (Fig. 6(C)).

ANOs-tFNA Complex Up-Regulated Apoptosis-Related Gene Expression

To explore the change in apoptosis-related genes expression after treatment with the ANOs-tFNA complex, Q-PCR was used to detect the expression of c-Met, Bax, and Caspase-3. After treatment for 24 h, we found that Bax and Caspase-3 were up-regulated significantly in

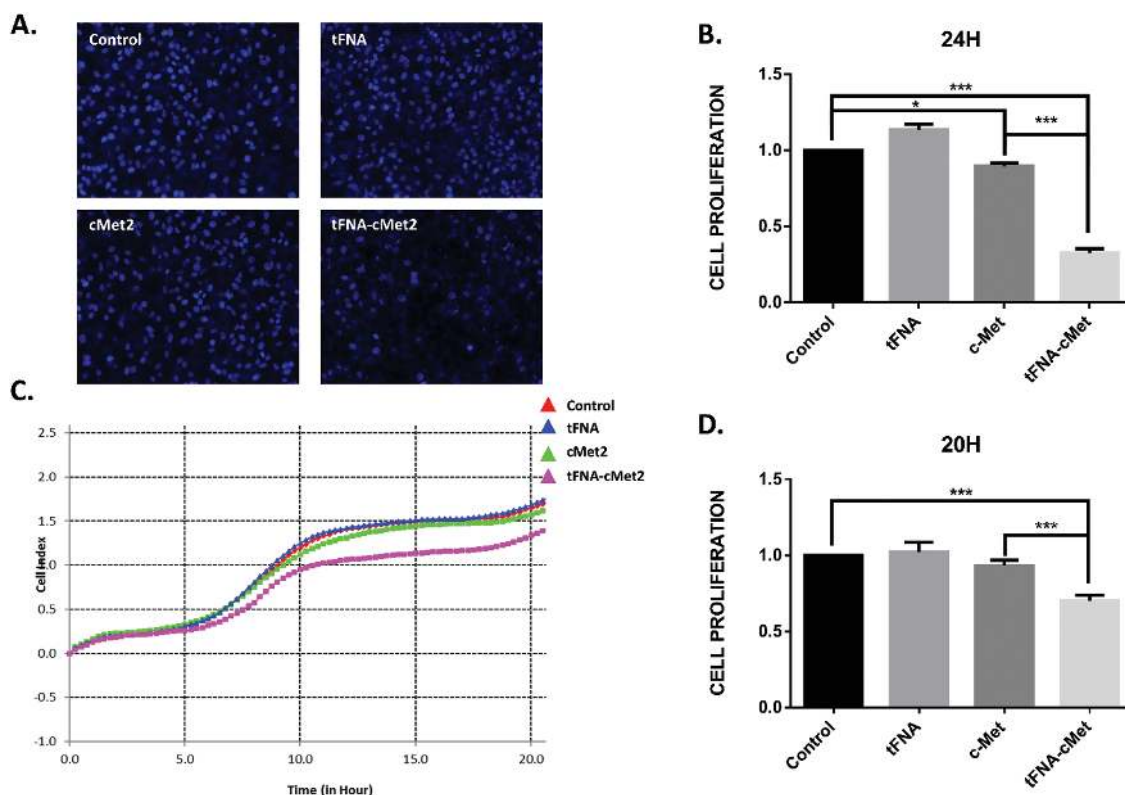


Figure 4. Influence of tFNA-ANOs complex on cell migration. (A) Migration-Transwell chamber assay was used to detect the effect of tFNA-ANOs complex on cell migration. Representative fluorescence images were taken after staining nuclei of the transmigrated cells with DAPI (magnification, 100x). (B) Statistical analysis was performed by counting cell number of migrate. Data are presented as mean \pm SD ($n = 4$). Statistical analysis: * $p < 0.05$, ** $p < 0.01$, *** $p < 0.001$. (C) Cell migration was detected by RTCA system. (D) Compared effect of different drugs (250 nM) on cell migration at 20 h. Data are presented as mean \pm SD ($n = 4$). Statistical analysis: * $p < 0.05$, ** $p < 0.01$, *** $p < 0.001$.

the tFNA-cMet group (Fig. 6(A)), which indicates that the ANOs-tFNA complex promoted cell apoptosis. Moreover, the level of c-Met was lower in the groups with ANOs-tFNA complex treatment than in the other groups (Fig. 6(A)). The result suggests that the ANOs-tFNA complex can inhibit TE10 cell proliferation and promote TE10 cell apoptosis.

Discussion

Antisense oligonucleotides are very promising drugs that can bind to specific mRNA strands to prevent genes from being translated into proteins to block the expression of the target genes [1–4]. However, their poor cell

uptake and easy degradability by nuclease limit their application [14–17]. In this study, we used tFNA, a kind of DNA-based nanostructure, for drug delivery applications. In contrast to ANOs, tFNA has been proven to enter cells more efficiently without any aid from transfection agents [27–32]. It has been reported that the over-expression of c-Met is related to the occurrence, development, invasion, metastasis, prognosis and drug resistance of a wide variety of tumors [7–10]. Therefore, we use tFNA to deliver ANOs targeting c-Met mRNA to silence the c-Met gene for cancer treatment. In conclusion, we successfully prepared the ANOs-tFNA complex and inhibited the proliferation and migration of tumor cells by

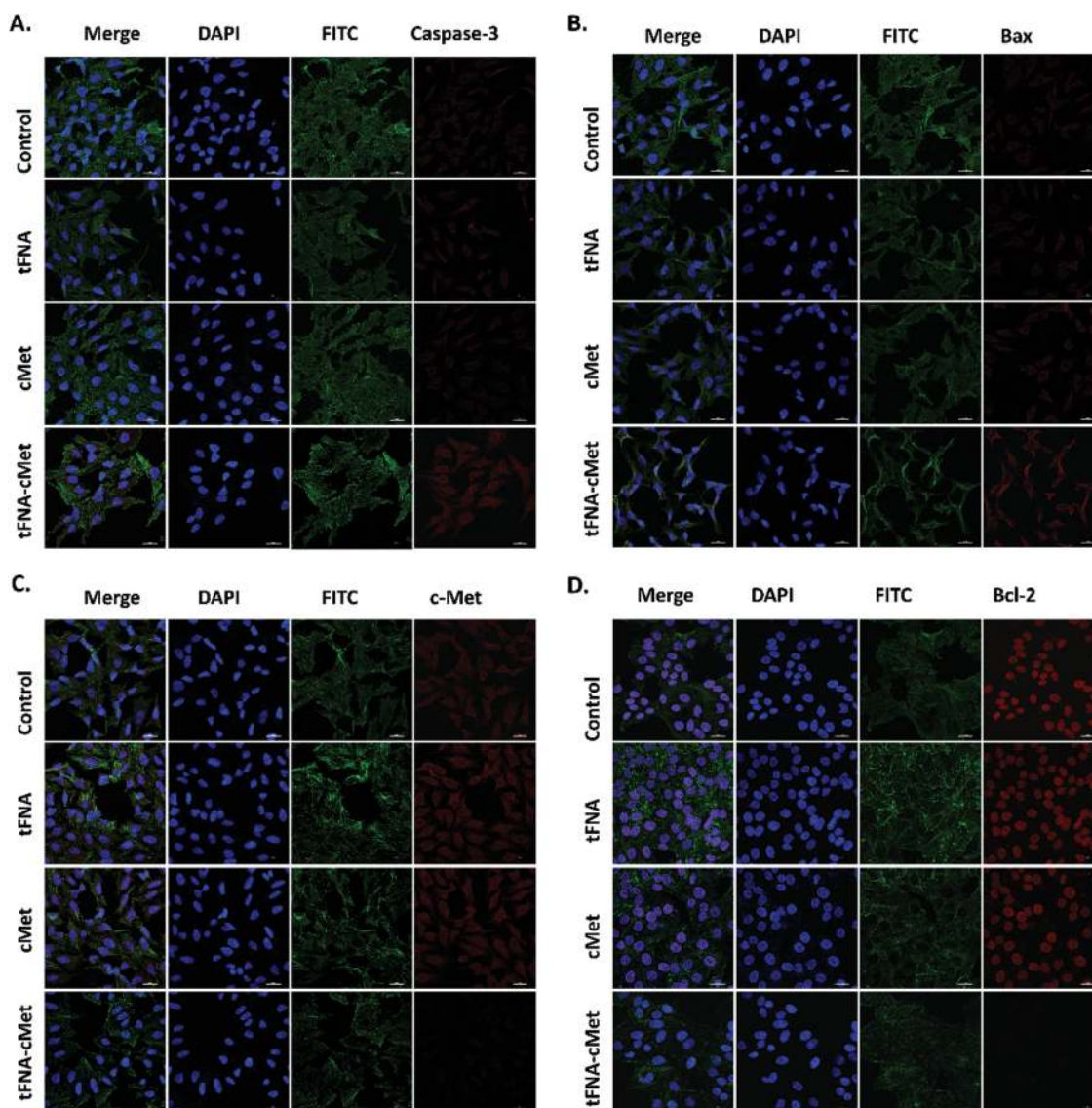


Figure 5. Apoptosis-related protein expression. (A, B) Caspase-3 and bax showed higher expression levels in tFNA-cMet group. Immunofluorescent images were taken to show the difference intuitively (protein: Red, cytoskeleton: Green and nucleus: Blue). Scale bars are 25 μm . (C, D) The expression of c-Met and Bcl-2 showed lower levels in tFNA-cMet group. Immunofluorescent images were taken to show the difference intuitively (protein: Red, cytoskeleton: Green and nucleus: Blue). Scale bars are 25 μm .

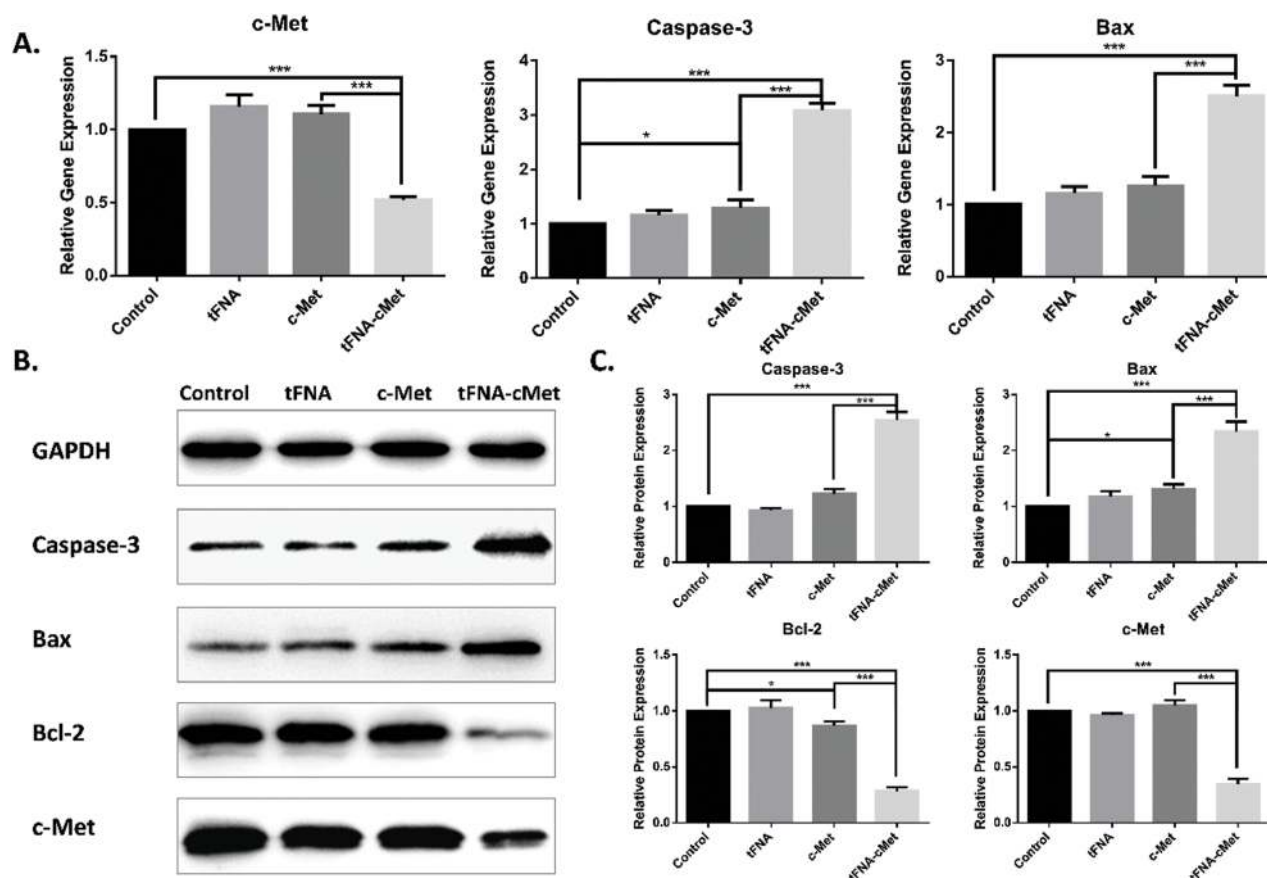


Figure 6. Apoptosis-related protein and gene expression. (A) Q-PCR analysis of bax, caspase-3, c-Met gene expression. Data are presented as mean \pm SD ($n = 4$). Statistical analysis: ** $p < 0.01$ and *** $p < 0.001$. (B) Western blot analysis of bax, bcl2, caspase3 and c-Met protein-expression. (C) Quantitative analysis of Western blot about bax, bcl2, caspase3 and c-Met protein-expression level. Data are presented as mean \pm SD ($n = 4$). Statistical analysis: ** $p < 0.01$ and *** $p < 0.001$.

blocking the HGF/c-Met molecular interaction and subsequent downstream signaling.

CONCLUSIONS

In this study, we conclude that tFNA are an excellent drug delivery vehicle because they can improve the cell uptake of ANOs targeting c-Met mRNA for cancer therapy. This research shows that tetrahedral FNAs can deliver functional antisense oligonucleotides into cells successfully through chemical modification for cancer therapy. It is well known that therapeutic nucleic acids, such as aptamers, antisense and siRNA, cannot enter cells without transfection agents, whereas tetrahedral FNAs can deliver these nucleic acids into cells. Therefore, tetrahedral FNAs are a promising carrier for intelligent drug delivery.

However, our study only focused on cell biological behavior *in vitro*, more *in vivo* researches are needed in the future. Additionally, in the future, we want to explore how tetrahedral FNAs can deliver other functional nucleic acids, such as PNAs, LNAs and siRNA.

As for drug delivery of tFNA, much remains to be explored.

Acknowledgments: This work was funded by the National Natural Science Foundation of China (81771125, 81471803).

REFERENCES

- Linnane, E., Davey, P. and Zhang, P., 2019. Differential uptake, kinetics and mechanisms of intracellular trafficking of next-generation antisense oligonucleotides across human cancer cell lines. *Nucleic Acids Research*, 47(9), pp.4375–4392.
- Jansen, B. and Zangemeister-Witke, U., 2002. Antisense therapy for cancer—The time of truth. *Lancet Oncology*, 3(11), pp.672–683.
- Tamm, I., Dörken, B. and Hartmann, G., 2001. Antisense therapy in oncology: New hope for an old idea? *Lancet Oncology*, 358(9280), pp.489–497.
- Xiong, Q.Q., Lee, G.Y. and Ding, J.X., 2018. Biomedical applications of mRNA nanomedicine. *Nano Research*, 11(10), pp.5281–5309.
- Sethi, N., and Kang, Y., 2011. Unravelling the complexity of metastasis-molecular understanding and targeted therapies. *Nature Reviews Cancer*, 11(10), pp.735–748.
- Chaffer, C.L. and Weinberg, R.A., 2011. A perspective on cancer cell metastasis. *Science*, 331(6024), pp.1559–1564.

7. Gherardi, E., Birchmeier, W. and Birchmeier, C., **2012**. Targeting MET in cancer: Rationale and progress. *Nature Reviews Cancer*, *12*(2), pp.89–103.
8. Hartmann, S., Bhola, N.E. and Grandis, J.R., **2016**. HGF/Met signaling in head and neck cancer: Impact on the tumor microenvironment. *Clinical Cancer Research*, *22*(16), pp.4005–4013.
9. Dai, L., Trillo-Tinoco, J. and Cao, Y., **2015**. Targeting HGF/c-MET induces cell cycle arrest, DNA damage, and apoptosis for primary effusion lymphoma. *Blood*, *126*(26), pp.2821–2831.
10. Maroun, C.R. and Rowlands, T., **2014**. The Met receptor tyrosine kinase: A key player in oncogenesis and drug resistance. *Journal of Pharmacology and Experimental Therapeutics*, *142*(3), pp.316–338.
11. Ueki, R. and Sando, S., **2014**. A DNA aptamer to c-Met inhibits cancer cell migration. *Chemical Communications (Cambridge, England)*, *50*(86), pp.13131–13134.
12. Sun, H., Chao, J. and Zuo, X., **2014**. Gold nanoparticle-decorated MoS₂ nanosheets for simultaneous detection of ascorbic acid, dopamine and uric acid. *Rsc Advances*, *4*(52), pp.27625–27629.
13. Lordick, F., **2014**. Targeting the HGF/MET pathway in gastric cancer. *Lancet Oncology*, *15*(9), pp.914–916.
14. Godfrey, C., Desviat, L.R. and Smedsrød, B., **2017**. Delivery is key: Lessons learnt from developing splice-switching antisense therapies. *EMBO Molecular Medicine*, *9*(5), pp.545–557.
15. Roh, Y.H., Lee, J.B. and Shopsowitz, K.E., **2014**. Layer-by-layer assembled antisense DNA microsphere particles for efficient delivery of cancer therapeutics. *ACS Nano*, *8*(10), pp.9767–9780.
16. Chen, J.J., Ding, J.X. and Xu, W.G., **2017**. Receptor and microenvironment dual-recognizable nanogel for targeted chemotherapy of highly metastatic malignancy. *Nano Letters*, *17*(7), pp.4526–4533.
17. Schoellhammer, C.M., Lauwers, G.Y. and Goettel, J.A., **2017**. Ultrasound-mediated delivery of RNA to colonic mucosa of live mice. *Gastroenterology*, *152*(5), pp.1151–1160.
18. Li, C., Faulkner-Jones, A., Dun, A.R., Jin, J., Chen, P., Xing, Y., Yang, Z., Li, Z., Shu, W., Liu, D. and Duncan, R.R., **2015**. Rapid formation of a supramolecular polypeptide-DNA hydrogel for *in situ* three-dimensional multilayer bioprinting. *Angewandte Chemie-International Edition*, *54*(13), pp.3957–3961.
19. Zuo, X.L., Peng, C. and Huang, Q., **2009**. Design of a carbon nanotube/magnetic nanoparticle-based peroxidase-like nanocomplex and its application for highly efficient catalytic oxidation of phenols. *Nano Research*, *2*(8), pp.617–623.
20. Zhang, Q., Jiang, Q., Li, N., Dai, L., Liu, Q., Song, L., Wang, J., Li, Y., Tian, J., Ding, B. and Du, Y., **2014**. DNA origami as an *in vivo* drug delivery vehicle for cancer therapy. *ACS Nano*, *8*(7), pp.6633–6643.
21. Wen, Y.L., Pei, H., Wan, Y., Su, Y., Huang, Q., Song, S.P. and Fan, C.H., **2011**. DNA nanostructure-decorated surfaces for enhanced aptamer target binding and electrochemical cocaine sensors. *Analytical Chemistry*, *83*(19), pp.7418–7423.
22. Li, Q.S., Zhao, D. and Shao, X.R., **2017**. Aptamer-modified tetrahedral DNA nanostructure for tumor-targeted drug delivery. *ACS Applied Materials & Interfaces*, *9*(42), pp.36695–36701.
23. Li, S.H., Tian, T.R., Zhang, T., Cai, X.X. and Lin, Y.F., **2018**. Advances in biological applications of self-assembled DNA tetrahedral nanostructures. *Materials Today*, *11*(24), pp.57–68.
24. Zhang, Y.X., Ma, W.J., Zhan, Y.X., Mao, C.C., Shao, X.R., Xie, X.P. and Lin, Y.F., **2018**. Nucleic acids and analogs for bone regeneration. *Bone Research*, *6*, p.37.
25. Li, J., Song, S.P. and Liu, X., **2008**. Enzyme-based multi-component optical nanoprobe for sequence-specific detection of DNA hybridization. *Advanced Materials*, *20*(3), p.497.
26. Lin, M.H., Wang, J.J. and Zhou, G., **2015**. Programmable engineering of a biosensing interface with tetrahedral DNA nanostructures for ultrasensitive DNA detection. *Angewandte Chemie-International Edition*, *54*(7), pp.2151–2155.
27. Guo, H., Xu, W.G. and Chen, J.J., **2017**. Positively charged polypeptide nanogel enhances mucoadhesion and penetrability of 10-hydroxycamptothecin in orthotopic bladder carcinoma. *Journal of Control Release*, *259*, pp.136–148.
28. Wen, Y.L., Pei, H. and Shen, Y., **2012**. DNA nanostructure-based interfacial engineering for PCR-free ultrasensitive electrochemical analysis of microRNA. *Scientific Reports*, *2*(1), p.867.
29. Liang, L., Li, J., Li, Q., Huang, Q., Shi, J., Yan, H. and Fan, C.H., **2014**. Single particle tracking and modulation of cell entry pathways of a tetrahedral DNA nanostructure in live cells. *Angewandte Chemie-International Edition*, *53*(30), pp.7745–7750.
30. Walsh, A.S., Yin, H., Erben, C.M., Wood, M.J. and Turberfield, A.J., **2011**. DNA cage delivery to mammalian cells. *ACS Nano*, *5*(7), pp.5427–5432.
31. Zhao, D., Liu, M.T., Li, Q.S., Xue, C.Y., Lin, Y.F. and Cai, X.X., **2018**. Tetrahedral DNA nanostructure promote endothelial cells proliferation, migration and angiogenesis via notch signaling pathway. *ACS Applied Materials & Interfaces*, *10*, pp.37911–37918.
32. Liu, N.X., Zhou, M., Zhang, Q., Yong, L., Zhang, T., Tian, T.R., Ma, Q.Q., Lin, S.Y., Zhu, B. and Cai, X.X., **2018**. Effect of substrate stiffness on proliferation and differentiation of periodontal ligament stem cells. *Cell Proliferation*, *51*(5), p.e12478.
33. Shao, X.R., Ma, W.J., Xie, X.P., Li, Q.S., Lin, S.Y., Zhang, T. and Lin, Y.F., **2018**. Neuroprotective effect of tetrahedral DNA nanostructures in a cell model of Alzheimer's disease. *ACS Applied Materials & Interfaces*, *10*, pp.23682–23692.
34. Zhao, D., Li, Q.S., Liu, M.T., Ma, W.J., Zhou, T., Xue, C.Y. and Cai X.X., **2018**. Substrate stiffness regulated migration and invasion ability of adenoid cystic carcinoma cells via RhoA/ROCK pathway. *Cell Proliferation*, *51*, p.e12442.
35. Ma, W.J., Shao, X.R., Zhao, D., Li, Q.S., Liu, M.T., Zhou, T., Xie, X.P., Mao, C.C., Zhang, Y.X. and Lin, Y.F., **2018**. Self-assembled tetrahedral DNA nanostructures promote neural stem cell proliferation and neuronal differentiation. *ACS Applied Materials & Interfaces*, *10*(9), pp.7892–7900.
36. He, Y., Zhong, Y.L. and Su, Y., **2011**. Water-dispersed near-infrared-emitting quantum dots of ultrasmall sizes for *in vitro* and *in vivo* imaging. *Angewandte Chemie-International Edition*, *50*(25), pp.5694–5697.
37. Fan, C.H., Zhuang, Y. and Li, G., **2000**. Direct electrochemistry and enhanced catalytic activity for hemoglobin in a sodium montmorillonite film. *Electroanalysis*, *12*(14), pp.1156–1158.
38. Shi, S.R., Lin, S.Y., Li, Y., Zhang, T., Shao, X.R., Tian, T.R., Zhou, T.F., Li, Q.S. and Lin, Y.F., **2018**. Effects of tetrahedral DNA nanostructures on autophagy in chondrocytes. *Chemical Communications (Cambridge, England)*, *54*(11), pp.1327–1330.
39. Zhang, Y., Wang, F., Li, M.Q., Yu, Z.Q., Qi, R.G., Ding, J.X., Zhang, Z.Y. and Chen, X.S., **2018**. Self-stabilized hyaluronate nanogel for intracellular codelivery of doxorubicin and cisplatin to osteosarcoma. *Advanced Science*, *5*(5), p.1700821.
40. Zhou, M., Liu, N.X., Shi S.R., Li, Y., Zhang, Q., Ma, Q.Q., Tian, T.R., Ma, W.J., Cai, X.X. and Lin, Y.F., **2018**. Effect of tetrahedral DNA nanostructures on proliferation and osteo/odontogenic differentiation of dental pulp stem cells via activation of the notch signaling pathway. *Nanomedicine: Nanotechnology, Biology, and Medicine*, *14*(4), pp.1227–1236.
41. Zhang, Y.X., Ma, W.J., Zhu, Y., Shi, S.R., Li, Q.S., Mao, C.C., Zhao, D., Zhan, Y.X., Shi, J.Y., Li, W., Wang, L.H., Fan, C.H. and Lin, Y.F., **2018**. Inhibiting methicillin-resistant *Staphylococcus aureus* by tetrahedral DNA nanostructure-enabled antisense peptide nucleic acid delivery. *Nano Letters*, *18*(9), pp.5652–5659.
42. Liu, M.T., Ma, W.J., Li, Q.S., Zhao, D., Shao, X.R., Huang, Q., Hao, L.Y. and Lin, Y.F., **2019**. Aptamer-targeted DNA nanostructures with doxorubicin to treat protein tyrosine kinase 7-positive tumors. *Cell Proliferation*, *52*(1), p.e12511.
43. Shi, S.R., Lin, S.Y., Shao, X.R., Li, Q.S., Zhang, T. and Lin, Y.F., **2017**. Modulation of chondrocyte motility by tetrahedral DNA nanostructures. *Cell Proliferation*, *50*(5), p.e12368.

44. Kashyap, M.K. and Abdel-Rahman, O., **2018**. Expression, regulation and targeting of receptor tyrosine kinases in esophageal squamous cell carcinoma. *Molecular Cancer*, *17*(1), p.54.
45. Catenacci, D.V., Tebbutt, N.C., Davidenko, I., Murad, A.M., Al-Batran, S.E., Ilson, D.H., Tjulandin, S., Gotovkin, E., Karaszewska, B., Bondarenko, I., Tejani, M.A., Udrea, A.A., Tehfe, M., De, V.F., Turkington, C., Tang, R., Ang, A., Zhang, Y., Hoang, T., Sidhu, R. and Cunningham, D., **2017**. Rilotumumab plus epirubicin, cisplatin, and capecitabine as first-line therapy in advanced MET-positive gastric or gastroesophageal junction cancer (RILOMET-1): A randomised, double-blind, placebo-controlled, phase 3 trial. *Lancet Oncology*, *18*(11), pp.1467–1482.
46. Catenacci, D.V., Ang, A., Liao, W.L., Shen, J., O'Day, E., Loberg, R.D., Cecchi, F., Hembrough, T., Ruzzo, A. and Graziano, F., **2017**. MET tyrosine kinase receptor expression and amplification as prognostic biomarkers of survival in gastroesophageal adenocarcinoma. *Cancer*, *123*(6), pp.1061–1070.
47. Bradley, C.A., Salto-Tellez, M., Laurent-Puig, P., Bardelli, A., Rolfo, C., Taberero, J., Khawaja, H.A., Lawler, M., Johnston, P.G., Van, S.S. and Mercuric, C., **2017**. Targeting c-MET in gastrointestinal tumors: Rationale, opportunities and challenges. *Nature Reviews Clinical Oncology*, *14*(9), pp.562–576.
48. Cai, X.X. and Xie, J., **2017**. Angiogenesis in a 3D model containing adipose tissue stem cells and endothelial cells is mediated by canonical Wnt signaling. *Bone Research*, *5*, p.17048.
49. Zhang, Q., Deng, S.W., Sun, K., Lin, S.Y., Lin, Y.F., Zhu, B.F. and Cai, X.X., **2017**. MMP-2 and Notch signal pathway regulate migration of adipose-derived stem cells and chondrocytes in co-culture systems. *Cell Proliferation*, *50*(6), p.e12385.

IP: 127.0.0.1 On: Thu, 05 Aug 2021 04:28:46
Copyright: American Scientific Publishers
Delivered by Ingenta